Supplement of Biogeosciences, 23, 4793–4820, 2026
https://doi.org/10.5194/bg-23-4793-2026-supplement

Biogeosciences
Open Access

Supplement of

New insights into the primary production and the structure of the phytoplankton community in the South Indian Ocean using size fractionation experiments

Valentin Deteix et al.

Correspondence to: Valentin Deteix (valentin.deteix@locean.ipsl.fr) and Céline Ridame (celine.ridame@locean.ipsl.fr)

S1. Choice of depth criterion for the productive layer in integration computations

For decades, oceanographers and marine biogeochemists have defined the depth of the productive layer (Z_{PL}) operationally. The most common criteria relies on irradiance from downcast profiles of photosynthetically active radiation (PAR), where Z_{PL} corresponds to the depth at which PAR is reduced to 1% of its surface value (Morel and Berthon, 1989; Ryther, 1956). Even though this definition has endured, it may not represent best the productive layer, as significant net primary production fluxes and chlorophyll *a* concentrations were previously reported below the 1% light level (*e.g.* Cavagna et al., 2015; Laws et al., 2014). Recently, Marra et al. (2023) compared several parameters to define Z_{PL} and concluded that the depth of the bottom of the fluorescence maximum was a good indicator of Z_{PL} and could be used over a broader range of trophic conditions. To define it, they used the intersection of two regression lines: one from the bottom of the profile and the other from the depth of the subsurface fluorescence maximum to the depth where fluorescence is at background. However, it was not evident in their example whether the intersection was clearly at the top of the fluorescence background or not. As acknowledged in their discussions: "Estimating this depth objectively is a difficult problem".

Based on this assessment, we defined our own criteria for the depth of bottom of the fluorescence maximum (Z_{FL}). Starting from the bottom of the fluorescence background, the objective was to determine the depth at which the fluorescence profile stands out from the background. We determined Z_{FL} to be the depth at which the fluorescence reaches the mean + 5 times the standard deviation of background fluorescence. The range for the background fluorescence values extended from 200 to 300 m for most of the SOCARB stations, but this range was adapted following each profile. Nevertheless, because irradiance is a more common feature to estimate Z_{PL}, we wanted to see if a specific irradiance value to define Z_{PL} could tend to Z_{FL}. When computing the depth of several euphotic layers – PAR at which PAR is reduced to 1%, 0.1% or 0.01% of its surface value: $Z_{EL1\%}$, $Z_{EL0.1\%}$ and $Z_{EL0.01\%}$ – we noted that Z_{FL} tended the most to $Z_{EL0.01\%}$ (Table S1a, Fig. S1). Furthermore, when comparing integrated total chlorophyll *a* for the total fraction (TChla_{TOTAL}) and for the size classes (TChla_{PICO}, TChla_{NANO}, TChla_{MICRO}) between Z_{FL} with $Z_{EL1\%}$, $Z_{EL0.1\%}$ and $Z_{EL0.01\%}$ (Table S1b), integrated TChl*a* with Z_{FL} exhibited the lowest relative differences with $Z_{EL0.01\%}$ (Table S1c), which justified our choice of $Z_{EL0.01\%}$ as the depth that best represents the depth of the productive layer (Table S1c).

S2. Use of primary production fluxes below the 1% surface PAR

Samples for NPP – and pigments – were collected at six depths between the surface (~ 10 m) and 200 m maximum. This range encompasses the euphotic layer at 1% of surface PAR, with NPP samples collected below $Z_{EL1\%}$. However, the set of available blue filters, used in the 24h incubations to simulate an irradiance level as close as possible to the sampled depth, ranged from 75 to 1% attenuation. This implies that for samples collected below $Z_{EL1\%}$, simulated irradiances during incubations were higher compared to *in situ* irradiance, and potentially leading to overestimated NPP fluxes below $Z_{EL1\%}$. We calculated the relative differences in integrated NPP over the $Z_{EL0.01\%}$ for the total fraction and the size classes, computed using all samples (0 samples excluded out of 12 stations) and computed using only the samples located above or close to $Z_{EL1\%}$ (20 samples excluded out of 72). The relative differences across the entire dataset were on average -5% ± 16%; more specifically, -6% ± 13% for the total fraction; -1% ± 15% for the pico-; -3% ± 14% for the nano- and -9% ± 20% for the microphytoplankton size fraction (Table S2). These average relative differences, which were negative and close to 0%, justified our choice to keep all NPP samples for the depth integration calculations.

S3. Detailed analysis of hydrographic fronts over the study area

On the north-south outward transect, the subtropical front (STF) was crossed between 41.20 and 41.50 °S and associated with a first and sharp decrease of SST and SSS (ΔSST = 6.62 °C per 100 km-1; ΔSSS = 1.883 PSU per 100 km-1). It was followed closely by the subantarctic front (SAF), crossed between 42.55 and 43.25°S and described with a second and sharp decrease of SST and SSS (ΔSST = 6.05 °C per 100 km-1; ΔSSS = 1.370 PSU per 100 km-1). The polar front (PF) was crossed between 52.54 and 52.82 °S and associated with a smaller SST gradient (ΔSST = 2.12 °C per 100 km-1). On the south-north return transect, the southern branch of the PF was crossed twice: once at station O10 (50.67 °S) where the temperature minimum at 200 m reached 2°C, and a second time between E (48.80 °S) and 47.18 °S (ΔSST = 1.71 °C per 100 km-1). The SAF was crossed between 46.27 and 45.65 °S (ΔSST = 5.28 °C per 100 km-1; ΔSSS = 1.042 PSU per 100 km-1), and the STF between 36.33 and 35.75 °S (ΔSST = 3.58 °C per 100 km-1; ΔSSS = 0.815 PSU per 100 km-1).

References

Cavagna, A. J., Fripiat, F., Elskens, M., Mangion, P., Chirurgien, L., Closset, I., Lasbleiz, M., Florez-Leiva, L., Cardinal, D., Leblanc, K., Fernandez, C., Lefèvre, D., Oriol, L., Blain, S., Quéguiner, B., and Dehairs, F.: Production regime and associated N cycling in the vicinity of

Kerguelen Island, Southern Ocean, Biogeosciences, 12, 6515–6528, https://doi.org/10.5194/bg-12-6515-2015, 2015.

Laws, E. A., Letelier, R. M., and Karl, D. M.: Estimating the compensation irradiance in the ocean: The importance of accounting for non-photosynthetic uptake of inorganic carbon, Deep Sea Research Part I: Oceanographic Research Papers, 93, 35–40, https://doi.org/10.1016/j.dsr.2014.07.011, 2014.

Marra, J. F., Chamberlin, W. S., Knudson, C. A., Rhea, W. J., and Ho, C.: Parameters for the depth of the ocean's productive layer, Frontiers in Marine Science, 10, https://doi.org/10.3389/fmars.2023.1052307, 2023.

Morel, A. and Berthon, J.-F.: Surface pigments, algal biomass profiles, and potential production of the euphotic layer: Relationships reinvestigated in view of remote-sensing applications, Limnology and Oceanography, 34, 1545–1562, https://doi.org/10.4319/lo.1989.34.8.1545, 1989.

Ryther, J. H.: Photosynthesis in the Ocean as a Function of Light Intensity, Limnology and Oceanography, 1, 61–70, https://doi.org/10.4319/lo.1956.1.1.0061, 1956.

Table S1. (a) Depths of the four different criteria used to integrate biogeochemical parameters (NPP): bottom of the fluorescence maximum (Z_{FL}), bottom of the euphotic layer for 1% ($Z_{EL1\%}$), 0.1% ($Z_{EL0.1\%}$) and 0.01% ($Z_{EL0.01\%}$) of the surface PAR value. Integrated TChl*a* (mg m^{-2}) for the total fraction and the size classes following four different depth criteria. (c) Relative differences between integrated TChl*a* over the Z_{FL} with those integrated over the $Z_{EL1\%}$, the $Z_{EL0.1\%}$ and the $Z_{EL0.01\%}$.

	O2	O3	O16	O14	O6	O7	O9	O12	E	A3	O10	O11
(a)												
Criteria depths [m]												
Z_{FL}	160	210	187	153	177	170	164	190	186	202	164	165
$Z_{EL1\%}$	93	118	90	87	84	82	83	46	63	48	69	101
$Z_{EL0.1\%}$	139	177	136	131	126	123	125	70	94	73	103	152
$Z_{EL0.01\%}$	185	236	181	174	168	164	167	93	125	97	137	203
(b)												
Integrated TChl*a*$_{PICO}$ [mg m^{-2}]												
∫ TChl*a*$_{PICO}$ over Z_{FL}	9.9	11.1	17.6	12.5	3.8	6.0	3.9	13.4	5.9	8.5	3.4	4.2
∫ TChl*a*$_{PICO}$ over $Z_{EL1\%}$	6.2	9.6	8.0	7.6	1.2	2.8	2.6	4.0	3.0	1.8	2.1	2.8
∫ TChl*a*$_{PICO}$ over $Z_{EL0.1\%}$	9.6	10.8	14.6	11.2	3.4	5.1	3.5	5.9	4.4	3.0	3.1	4.0
∫ TChl*a*$_{PICO}$ over $Z_{EL0.01\%}$	10.0	11.3	17.3	13.8	3.7	6.0	3.9	8.2	5.0	5.3	3.3	4.8
Integrated TChl*a*$_{NANO}$ [mg m^{-2}]												
∫ TChl*a*$_{NANO}$ over Z_{FL}	11.4	14.9	9.0	11.1	19.8	23.8	13.4	18.8	14.1	28.8	10.3	11.7
∫ TChl*a*$_{NANO}$ over $Z_{EL1\%}$	6.6	12.6	4.8	7.6	10.9	13.5	10.0	8.0	8.4	10.1	6.3	9.6
∫ TChl*a*$_{NANO}$ over $Z_{EL0.1\%}$	11.0	14.5	7.5	10.2	17.2	20.8	12.6	13.5	12.2	15.5	9.1	11.7
∫ TChl*a*$_{NANO}$ over $Z_{EL0.01\%}$	11.6	15.3	8.8	11.9	19.5	23.7	13.4	16.7	13.1	21.3	10.0	11.8
Integrated TChl*a*$_{MICRO}$ [mg m^{-2}]												
∫ TChl*a*$_{MICRO}$ over Z_{FL}	3.4	6.1	5.9	7.4	17.0	8.9	10.8	39.4	27.9	60.8	22.9	8.6
∫ TChl*a*$_{MICRO}$ over $Z_{EL1\%}$	1.8	5.2	4.2	6.4	9.2	3.1	8.2	20.0	15.2	21.0	13.6	6.7
∫ TChl*a*$_{MICRO}$ over $Z_{EL0.1\%}$	3.2	6.0	5.6	7.2	15.8	7.1	10.3	28.6	22.5	30.8	20.0	8.5
∫ TChl*a*$_{MICRO}$ over $Z_{EL0.01\%}$	3.5	6.2	5.8	7.6	16.9	8.9	10.8	33.3	24.9	39.2	22.1	8.9
Integrated TChl*a*$_{TOTAL}$ [mg m^{-2}]												
∫ TChl*a*$_{TOTAL}$ over Z_{FL}	24.8	32.1	32.5	31.0	40.6	38.7	28.0	71.7	48.0	98.2	36.5	24.5
∫ TChl*a*$_{TOTAL}$ over $Z_{EL1\%}$	14.6	27.3	17.0	21.6	21.3	19.5	20.8	31.9	26.6	32.9	22.0	19.1
∫ TChl*a*$_{TOTAL}$ over $Z_{EL0.1\%}$	23.7	31.3	27.8	28.7	36.5	33.0	26.4	48.0	39.2	49.3	32.1	24.1
∫ TChl*a*$_{TOTAL}$ over $Z_{EL0.01\%}$	25.1	32.8	31.9	33.3	40.1	38.5	28.1	58.2	43.1	65.7	35.4	25.5
(c)												
Δ of integrated TChl*a*$_{PICO}$ [%]												
Δ ($Z_{FL} - Z_{EL1\%}$)	-38	-14	-55	-39	-68	-53	-34	-70	-49	-79	-37	-34
Δ ($Z_{FL} - Z_{EL0.1\%}$)	-4	-3	-17	-10	-8	-16	-10	-56	-26	-64	-10	-5
Δ ($Z_{FL} - Z_{EL0.01\%}$)	1	2	-2	10	0	-1	1	-39	-16	-38	-2	14
Δ of integrated TChl*a*$_{NANO}$ [%]												
Δ ($Z_{FL} - Z_{EL1\%}$)	-42	-16	-47	-31	-45	-43	-25	-58	-41	-65	-39	-18
Δ ($Z_{FL} - Z_{EL0.1\%}$)	-4	-3	-17	-7	-13	-13	-6	-28	-13	-46	-12	0
Δ ($Z_{FL} - Z_{EL0.01\%}$)	1	2	-2	7	-2	0	0	-11	-7	-26	-3	1
Δ of integrated TChl*a*$_{MICRO}$ [%]												
Δ ($Z_{FL} - Z_{EL1\%}$)	-46	-15	-28	-14	-46	-65	-23	-49	-45	-66	-41	-22
Δ ($Z_{FL} - Z_{EL0.1\%}$)	-6	-2	-5	-3	-7	-20	-4	-27	-19	-49	-13	-1
Δ ($Z_{FL} - Z_{EL0.01\%}$)	4	2	-1	3	-1	0	0	-16	-11	-36	-3	4
Δ of integrated TChl*a*$_{TOTAL}$ [%]												
Δ ($Z_{FL} - Z_{EL1\%}$)	-41	-15	-48	-30	-47	-50	-26	-55	-44	-66	-40	-22
Δ ($Z_{FL} - Z_{EL0.1\%}$)	-4	-3	-15	-8	-10	-15	-6	-33	-18	-50	-12	-1
Δ ($Z_{FL} - Z_{EL0.01\%}$)	1	2	-2	7	-1	0	0	-19	-10	-33	-3	4

Table S2. Comparison of integrated net primary production (NPP) following two different methods sharing the same depth criterion ($Z_{EL0.01\%}$): the first method [1] remaining usual (0 samples excluded) and the second method [2] where samples above or close to $Z_{EL1\%}$ were kept to compute the integration (20 samples excluded).

	O2	O3	O16	O14	O6	O7	O9	O12	E	A3	O10	O11
Integrated NPP [mgC m^{-2} d^{-1}]												
[1] Classic method: ∫ PP over $Z_{EL0.01\%}$ (0 samples excluded out of 72)												
∫ PP_{PICO}	111	182	117	255	44	54	47	70	41	60	39	34
∫ PP_{NANO}	361	714	109	568	351	430	313	308	408	490	210	271
∫ PP_{MICRO}	87	277	336	649	669	671	641	3227	865	1571	671	233
∫ PP_{TOTAL}	559	1173	562	1472	1064	1155	1002	3605	1314	2120	921	537
Integrated NPP [mgC m^{-2} d^{-1}]												
[2] Alternative method: ∫ PP over $Z_{EL0.01\%}$ and keeping samples above or close to $Z_{EL1\%}$ (20 samples excluded out of 72)												
∫ PP_{PICO}	139	190	125	255	54	45	56	62	37	57	33	29
∫ PP_{NANO}	452	848	138	568	378	345	341	291	375	458	199	265
∫ PP_{MICRO}	108	280	385	649	708	814	677	2524	974	1319	734	365
∫ PP_{TOTAL}	698	1318	648	1472	1141	1204	1073	2877	1385	1834	966	659
Δ (∫ $NPP_{[1]}$ – ∫ $NPP_{[2]}$) [%]												
∫ PP_{PICO}	-25	-4	-7	0	-24	17	-18	11	10	4	15	13
∫ PP_{NANO}	-25	-19	-26	0	-8	20	-9	5	8	6	5	2
∫ PP_{MICRO}	-24	-1	-15	0	-6	-21	-6	22	-13	16	-9	-57
∫ PP_{TOTAL}	-25	-12	-15	0	-7	-4	-7	20	-5	13	-5	-23

Table S3. Relative contributions of each size class to integrated total chlorophyll *a* (∫TChl*a*) and integrated net primary production (∫NPP) over the $Z_{EL0.01\%}$. Stations were grouped according to their hydrographic zone and biogeochemical region.

St.	Zone	Region	∫TChl*a* [%]			∫NPP [%]		
			Pico-	Nano-	Micro-	Pico	Nano	Micro
Subtropical Zone								
O2	STZ	LNLC	40	46	14	20	65	16
O3	STZ	LNLC	35	46	19	16	61	24
O16	STZ	LNLC	54	28	18	21	19	60
Mean ± SD			43 ± 10	40 ± 11	17 ± 3	19 ± 3	48 ± 25	33 ± 24
Subantarctic Zone								
O14	SAZ	HN-LSi-LC	41	36	23	17	39	44
Polar Frontal Zone – offshore								
O6	PFZ	HN-LSi-LC	9	49	42	4	33	63
O7	PFZ	HN-LSi-LC	15	61	23	5	37	58
O9	PFZ	HN-LSi-LC	14	48	38	5	31	64
Mean ± SD			13 ± 3	53 ± 8	35 ± 10	4 ± 0	34 ± 3	62 ± 3
Kerguelen bloom region								
O12	PFZ	KER (PFZ)	14	29	57	2	9	90
E	AZ	KER (AZ)	12	30	58	3	31	66
A3	AZ	KER (AZ)	8	32	60	3	23	74
Mean ± SD			11 ± 3	31 ± 2	58 ± 1	3 ± 1	21 ± 11	76 ± 12
Antarctic Zone – offshore								
O10	AZ	HNLC	9	28	62	4	23	73
O11	AZ	HNLC	19	46	35	6	50	43
Mean			14	37	49	5	37	58
Global study area								
Mean ± SD			23 ± 16	40 ± 11	37 ± 18	9 ± 7	35 ± 17	56 ± 21

STZ, Subtropical Zone; SAZ, Subantarctic Zone; PFZ, Polar Frontal Zone; AZ, Antarctic Zone; KER, Kerguelen bloom; TChla, total chlorophyll a; PP, Primary production.

Table S4. Relative contributions of integrated pigments (%) over the $Z_{EL\ 0.01\%}$ for each size class.

Pigment	O2	O3	O16	O14	O6	O7	O9	O12	E	A3	O10	O11
Fucoxanthin												
Fuco $_{PICO}$	20	20	48	24	4	12	6	5	5	6	3	6
Fuco $_{NANO}$	39	35	33	22	24	42	22	12	15	17	11	29
Fuco $_{MICRO}$	41	45	19	54	72	46	71	83	80	77	86	65
Peridinin												
Peri $_{PICO}$	0	0	4	2	2	3	3	0	2	0	1	0
Peri $_{NANO}$	62	50	33	31	42	50	23	13	36	38	11	51
Peri $_{MICRO}$	38	50	63	66	56	47	74	87	63	62	88	49
19'-hexanoyloxyfucoxanthin												
Hex-fuco $_{PICO}$	6	9	33	33	6	13	15	20	16	9	16	28
Hex-fuco $_{NANO}$	72	61	33	38	68	68	71	43	47	41	56	64
Hex-fuco $_{MICRO}$	22	30	34	29	26	18	14	37	37	50	28	8
19'-butanoyloxyfucoxanthin												
But-fuco $_{PICO}$	25	31	60	59	12	15	25	29	24	19	20	37
But-fuco $_{NANO}$	54	50	22	28	65	60	56	52	46	41	38	49
But-fuco $_{MICRO}$	21	18	18	13	23	25	18	19	31	40	42	14
Alloxanthin												
Allo $_{PICO}$	0	0	24	29	7	11	18	25	27	10	27	12
Allo $_{NANO}$	68	79	35	44	68	73	72	69	60	55	63	80
Allo $_{MICRO}$	32	21	41	27	25	15	10	6	13	36	10	8
Chlorophyll *b*												
Chl*b* $_{PICO}$	56	34	43	24	30	23	41	53	41	42	23	69
Chl*b* $_{NANO}$	37	55	46	59	45	64	49	45	26	41	36	20
Chl*b* $_{MICRO}$	7	11	11	17	25	13	11	2	33	18	41	11
Zeaxanthin												
Zea $_{PICO}$	84	86	85	82	28	35	45	54	72	63	65	84
Zea $_{NANO}$	15	12	13	18	62	59	50	44	19	30	34	14
Zea $_{MICRO}$	1	2	2	0	10	7	5	0	10	7	1	2
Divinyl-chlorophyll *a*												
DVChl*a* $_{PICO}$	86	87	86	70	NA	NA	NA	NA	NA	NA	NA	NA
DVChl*a* $_{NANO}$	13	10	10	13	NA	NA	NA	NA	NA	NA	NA	NA
DVChl*a* $_{MICRO}$	1	3	4	16	NA	NA	NA	NA	NA	NA	NA	NA

Table S5. Average (mean ± SD) integrated biomass over the $Z_{EL0.01\%}$ with their relative contribution to TChla_{TOTAL} of each phytoplankton chemotaxonomic groups found in the micro-, nano- and picophytoplankton size classes (n = 12) over the study area.

Phytoplankton group	Integrated biomass [mg m^{-2}]			Relative contribution to TChla_{TOTAL} [%]		
	Micro-	Nano-	Pico-	Micro-	Nano-	Pico-
Diatoms	7.73 ± 6.91	2.28 ± 1.65	0.43 ± 0.53	20.3 ± 18.1	6.0 ± 4.3	1.1 ± 1.4
Haptophytes	5.28 ± 4.26	7.21 ± 2.74	2.46 ± 1.35	13.8 ± 11.2	18.9 ± 7.2	6.5 ± 3.5
Cryptophytes	0.31 ± 0.60	0.59 ± 0.57	0.24 ± 0.23	0.8 ± 1.6	1.5 ± 1.5	0.6 ± 0.6
Dinoflagellates	1.07 ± 0.94	1.51 ± 1.41	0.05 ± 0.05	2.8 ± 2.5	4.0 ± 3.7	0.1 ± 0.1
Chlorophytes	0.44 ± 0.41	1.93 ± 1.44	0.94 ± 0.65	1.2 ± 1.1	5.1 ± 3.8	2.5 ± 1.7
Pelagophytes	0.62 ± 0.37	0.82 ± 0.68	1.13 ± 1.02	1.6 ± 1.0	2.2 ± 1.8	3.0 ± 2.7
Synechococcus	0.18 ± 0.24	0.19 ± 0.21	0.83 ± 1.07	0.5 ± 0.6	0.5 ± 0.5	2.2 ± 2.8
Prochlorococcus	0.06 ± 0.10	0.21 ± 0.38	1.64 ± 2.89	0.2 ± 0.3	0.6 ± 1.0	4.3 ± 7.6

Table S6. Integrated nutrients concentrations over the $Z_{EL0.01\%}$. Stations were grouped according to their hydrographic zone and biogeochemical region. Integrated nutrients are rounded to the nearest 5 for a better readability.

St.	Zone	Region	∫Nutrients [mmol m^{-2}]		
			NO_X	DIP	DSi
O2	STZ	LNLC	390	45	520
O3	STZ	LNLC	840	75	775
O16	STZ	LNLC	720	70	435
O14	SAZ	HN-LSi-LC	1020	85	470
O6	PFZ	HN-LSi-LC	3945	270	1620
O7	PFZ	HN-LSi-LC	3555	245	1080
O9	PFZ	HN-LSi-LC	4260	290	1870
O12	PFZ	KER (PFZ)	1760	130	270
E	AZ	KER (AZ)	2380	165	1210
A3	AZ	KER (AZ)	2275	165	475
O10	AZ	HNLC	3480	235	1510
O11	AZ	HNLC	5845	405	6025

STZ, Subtropical Zone; SAZ, Subantarctic Zone; PFZ, Polar Frontal Zone; AZ, Antarctic Zone; KER, Kerguelen bloom; $NO_X = NO_3^- + NO_2^-$; DIP, dissolved inorganic phosphorus; DSi, dissolved silicon

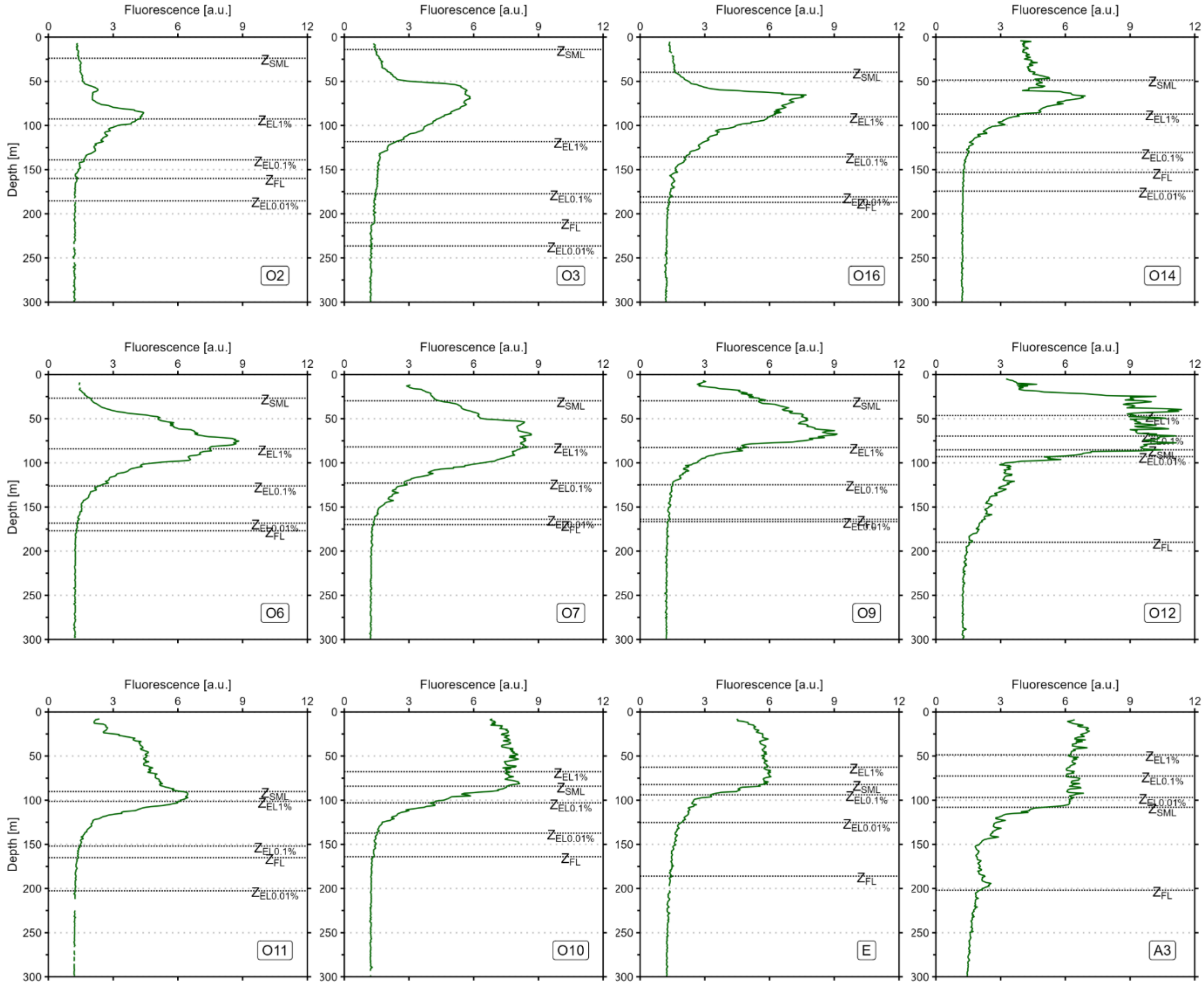

Figure S1. Vertical profiles of fluorescence (arbitrary unit) at the SOCARB stations. The dashed lines represent the depth of the surface mixed layer (Z_{SML}), the depth of the euphotic layer for 1% ($Z_{EL1\%}$), 0.1% ($Z_{EL0.1\%}$) and 0.01% and ($Z_{EL0.01\%}$), and the depth of bottom of the fluorescence maximum (Z_{FL}).

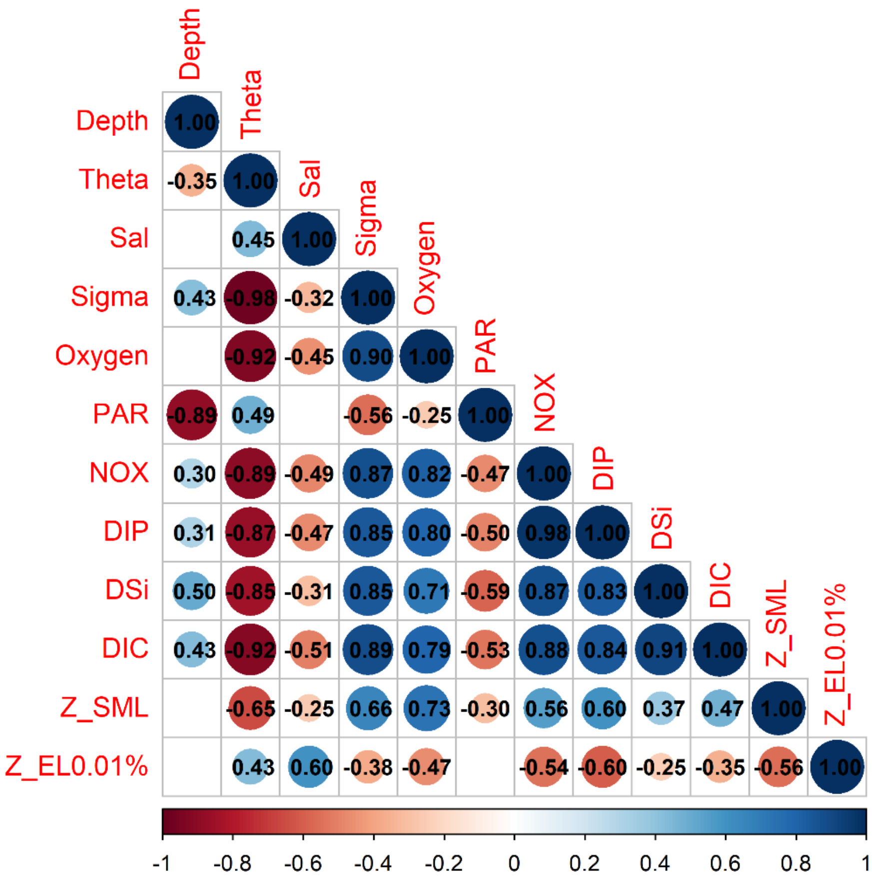

Figure S2. Heatmap of Spearman correlations between environmental variables selected in the principal component analysis. Only significant correlations with a threshold of $p < 0.05$ are displayed.

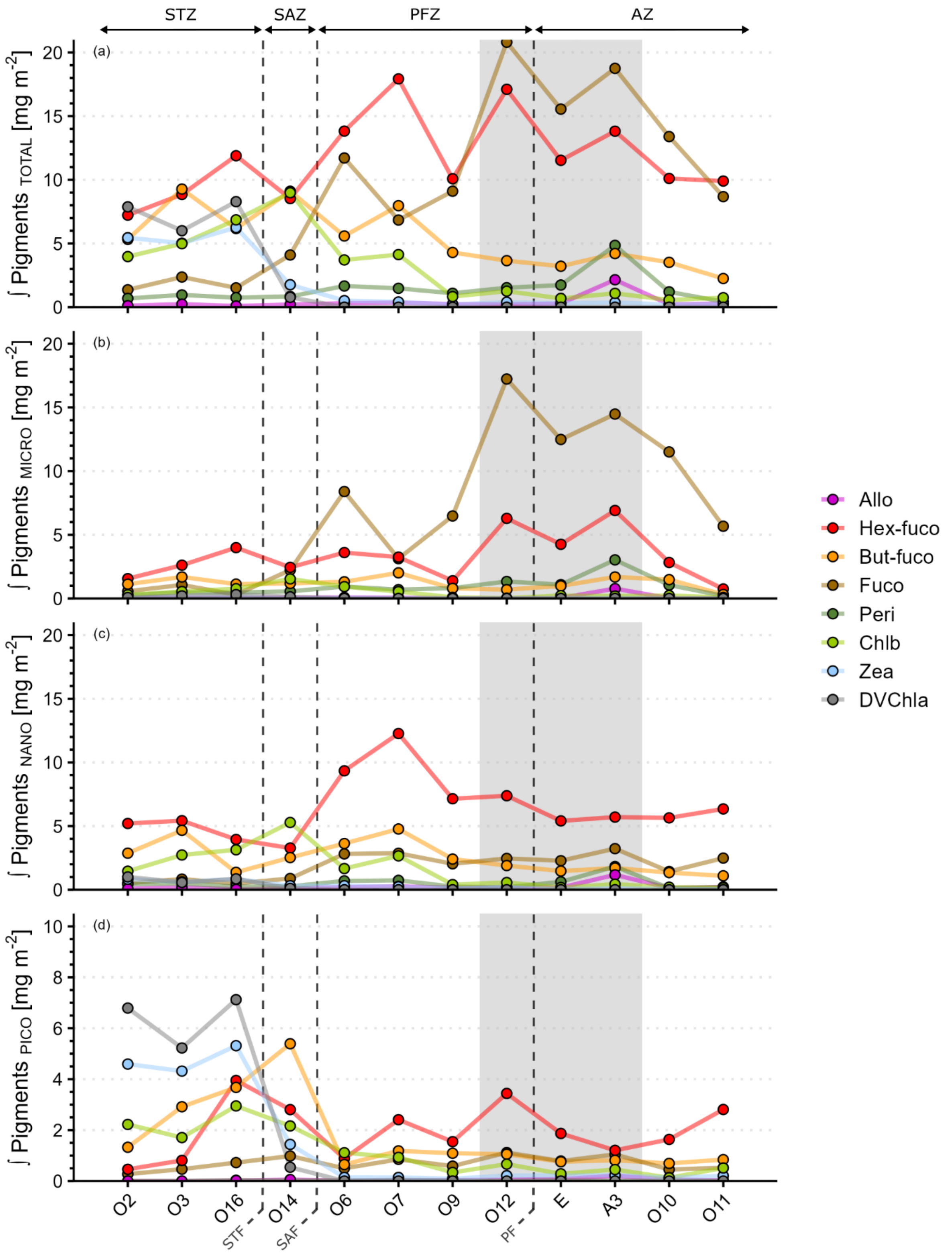

Figure S3. Spatial distribution of the main integrated pigment concentrations (∫ Pigments) over the $Z_{EL0.01\%}$ for (a) the whole community, (b) the micro-, (c) the nano- and (d) the picophytoplankton size classes. Mind the y-axis scale differences for the picophytoplankton panel compared to the others. Stations were grouped according to their hydrographic zone and biogeochemical region. The grey box covers the stations in the Kerguelen region. The dotted lines represent the main Southern Ocean fronts: STF, Subtropical Front; SAF, Subantarctic Front; PF, Polar Front. STZ, Subtropical Zone; SAZ, Subantarctic Zone; PFZ, Polar Frontal Zone; AZ, Antarctic Zone.

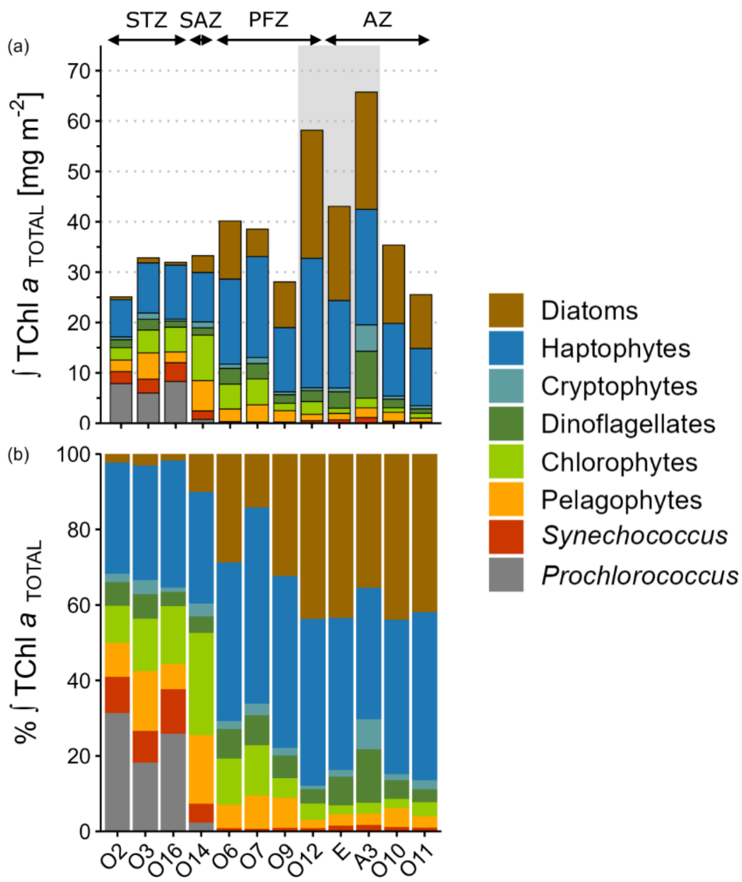

Figure S4. Spatial distribution of phytoplankton taxonomic groups of (a) integrated TChl*a* and (b) relative contribution to integrated TChl*a* over the $Z_{EL0.01\%}$ for the total fraction. Note that the total fraction data results from the sum of the phytoplankton chemotaxonomic groups biomass for each size class.

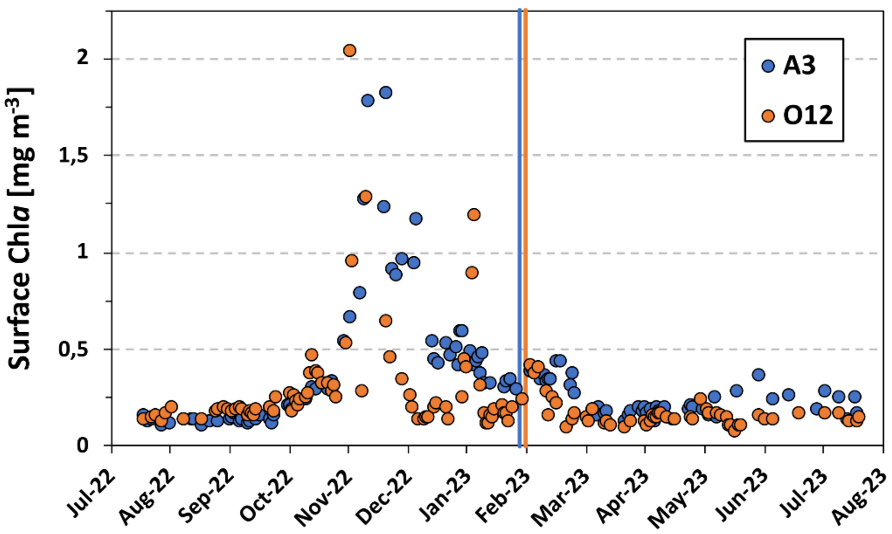

Figure S5. Surface chlorophyll *a* phenology at A3 (blue) and O12 (orange) from Aug. 2022 to Aug. 2023 (Copernicus-GlobColour L3 daily satellite product). The horizontal lines represent the sampling date for each station.